

Asymptotic analysis of cross-hole pneumatic injection tests in unsaturated fractured tuff

Walter A. Illman^{a,b,*}, Daniel M. Tartakovsky^c

^a Department of Geoscience, University of Iowa, Iowa City, IA 52242-1379, USA

^b Department of Civil and Environmental Engineering, and IHR-Hydroscience and Engineering, University of Iowa, Iowa City, IA 52242, USA

^c Theoretical Division, Los Alamos National Laboratory, Los Alamos, NM 87545, USA

Received 26 August 2004; received in revised form 23 February 2005; accepted 14 March 2005

Available online 4 June 2005

Abstract

We present a new method to interpret three-dimensional pressure interference tests, which is based on an asymptotic analysis of late time pressure transient data. The approach yields reliable estimates of equivalent permeability and porosity without resorting to type-curve fitting or numerical inverse models. This is accomplished by analyzing the late-time behavior of type-curve solutions for pressure interference tests. We use our approach to infer the permeability and porosity of fractured tuff from cross-hole pneumatic injection test data. Their values are found to be in good agreement with those inferred from more complicated methods of data analysis. We analyze the statistical properties of the estimated equivalent permeability and porosity and observe a weak correlation between the two.

© 2005 Elsevier Ltd. All rights reserved.

Keywords: Permeability; Porosity; Pneumatic injection test; Well-test analysis; Fracture flow; Scale effect; Straight-line analysis; Asymptotic analysis

1. Introduction

Well testing is routinely used to identify hydraulic parameters of the subsurface, e.g., hydraulic conductivity, porosity, and permeability. These tests infer such parameters indirectly by relying on mathematical models to relate them to measured quantities, such as drawdown and flow rate. While numerical inversion of flow equations can be used to achieve this goal, it is often complex, computationally expensive, and plagued by the issues of non-uniqueness. These are some of the reasons why analytical techniques, which include transient type-curve, semi-log, and steady-state analyses, remain the method of choice in well test analysis. On the other

hand, analytical solutions rely on a number of simplifying assumptions, such as subsurface homogeneity or perfect layering.

Type-curve analyses have been used extensively to infer equivalent hydraulic parameters from transient well tests. The use of early time data to match type curves often violate the assumption of homogeneity, on which most of these analyses are based. It can also be problematic, since borehole storage and other near-well effects often render early-time data not representative of an aquifer's properties on the measurement scale. Finally, early-time data are often noisy and strongly affected by external forcings, such as barometric pressure fluctuations.

The use of late-time and steady-state data to infer the parameters of heterogeneous media from homogeneous models might be more appropriate, since pressure transients propagate through a large portion of the investigated region leading to an effective spatial averaging.

* Corresponding author. Address: Department of Geoscience, University of Iowa, Iowa City, IA 52242-1379, USA.

E-mail addresses: walter-illman@uiowa.edu (W.A. Illman), dmt@lanl.gov (D.M. Tartakovsky).

For example, the use of steady-state data to analyze a large number of cross-hole pneumatic injection tests made it possible to interpret the experiments that were not analyzable by type-curve methods due to the departure of early data from the type curves due to near-well heterogeneities [1].

A downside of relying on steady-state analyses stems from the fact that under field conditions a steady-state regime might be difficult to achieve and the pressure interference tests may have to be run for an exceedingly long time. In fact, well tests often do not reach steady-state regimes at all. In addition, the steady-state analyses of pressure interference tests do not allow one to infer equivalent porosity.

Recently, we [2] proposed a new approach to well test analysis, which overcomes many of these difficulties by providing reliable estimates of equivalent permeability and porosity without resorting to type curves or numerical inverse models. Instead, the approach relies on an asymptotic analysis of the late-time behavior of the analytical solution [3] for cross-hole tests, in which both injection and monitoring intervals are treated as points. The advantages of this approach are twofold. First, since it results in the so-called straight-line data analysis, it is easy to implement and less prone to interpretive errors than its curve-fitting counterparts. Second, since this approach does not utilize early-time data, it is less affected by local heterogeneities, thus producing more reliable estimates of equivalent permeability and porosity on the scale of the experiment.

The main goal of this study is to extend and generalize the asymptotic analysis [2] of cross-hole pneumatic injection tests by incorporating the geometric relationship between injection and monitoring intervals. This is crucial for the interpretation of data collected from tests with long injection and/or monitoring intervals, which are located close to each other. In Section 2, we derive new asymptotic solutions for cross-hole test in which the injection interval can be treated as either a point or a line source, while the monitoring interval is treated as a line. These solutions are used in Section 3 to infer the equivalent permeability and porosity of fractured tuff at the Apache Leap Research Site near Superior, Arizona [4,5]. In Section 4 we compare these estimates with the estimates of equivalent permeability and porosity obtained from the type-curve [6] steady-state [1] and numerical inverse [7] analyses, and comment on the relative advantages of the proposed methodology. Finally, the correlation between the equivalent permeabilities and porosities is examined in Section 5.

2. Methodology

Cross-hole pneumatic tests in unsaturated porous and fractured media consist of injecting air through a

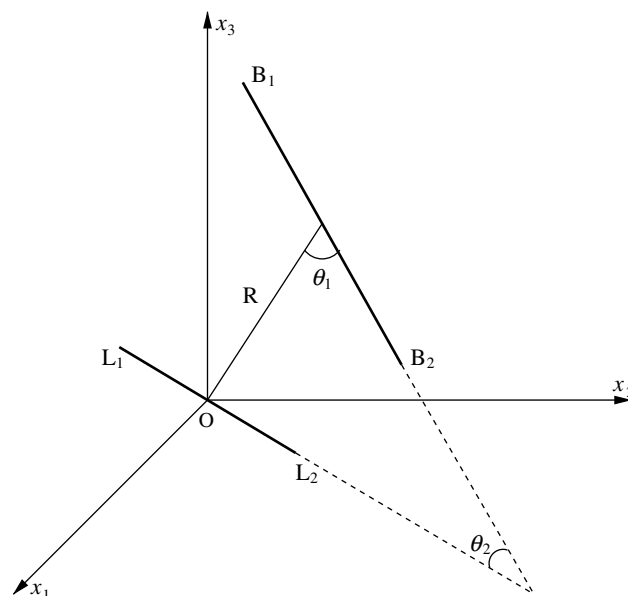


Fig. 1. A schematic representation of a cross-hole injection test. The lengths of injection (L_1, L_2) and monitoring (B_1, B_2) intervals are L and B , respectively. The centroid of the former coincides with the origin of the coordinate system, while the centroid of the latter is located the distance R away. The angle between the line connecting the two centroids and the monitoring interval is θ_1 , and the angle between the injection and monitoring intervals is θ_2 .

well and monitoring pressure transients in observation wells (Fig. 1). This induces flow of air and water that can be described by two-phase flow equations that can exhibit non-Darcian behavior at high Reynolds numbers. The development of the corresponding analytical type-curve analyses [6] requires that two-phase flow equations be approximated with single-phase airflow equations by treating water as immobile. The airflow equation must additionally be linearized leading to solutions in terms of pressure, p , as is customary for liquids or in terms of pressure-squared, p^2 , as is common for gases [6,8]. Since the alternative interpretations of single-hole [8] and cross-hole [6] pneumatic injection based on either p^2 or p formulations of type-curve solutions lead to similar estimates of permeability and porosity, we adopt a simpler p -based representation.

Within this framework, airflow is described by the standard diffusion equation and type-curve solutions for pumping tests in fully saturated aquifers apply. In particular, here we are concerned with a series solutions for cross-hole well-test analysis [3]. To simplify the presentation, we treat the subsurface as isotropic. The incorporation of anisotropy into the results presented here is relatively straightforward [2]. Specifically, we derive asymptotic solutions for tests with (i) a point-injection and line-observation intervals (a point-to-line solution), and (ii) line-injection and line-observation intervals (a line-to-line solution). For completeness, we

also present a solution for point-injection and point-observation intervals (a point-to-point solution) [2].

In all three asymptotic solutions, pressure p varies linearly with $1/\sqrt{t_d}$, where t_d is dimensionless time, so that late-time pressure data are amenable to the so-called straight-line analysis when plotted against $1/\sqrt{t_d}$. This is conceptually similar to the Jacob’s method of analysis of the Theis solution [9], wherein pressure data are plotted against $\log t_d$.

It is important to note that while we formulate these solutions in terms relevant to pneumatic pressure transient tests in unsaturated geologic media, they are also valid for pressure interference tests in saturated aquifers when written in terms of hydraulic head.

2.1. Point-to-point solution

A full solution for a point source ($|L_1L_2| \equiv L = 0$ and $|B_1B_2| \equiv B = 0$ in Fig. 1) in an infinite three-dimensional isotropic homogeneous medium is given by [3, Eqs. (7)–(9)]

$$p_d(t_d) = \operatorname{erfc}\left(\frac{1}{\sqrt{4t_d}}\right), \tag{1}$$

where the dimensionless pressure drop in the monitoring interval and time are given by

$$p_d = \frac{4\pi kRp}{q\mu} \quad \text{and} \quad t_d = \frac{kt p_{\text{ave}}}{\phi\mu R^2}, \tag{2}$$

respectively. Here R is the distance between the centroids of the injection and monitoring intervals, t is time, p is pressure, k is intrinsic permeability, q is flow rate, μ is the dynamic viscosities of air, p_{ave} is average pressure, and ϕ is porosity.

An asymptotic expansion of (1) for large time t_d gives [2]

$$p = \frac{q\mu}{4\pi kR} - \frac{q\mu}{4\sqrt{\pi}k} \sqrt{\frac{\phi\mu}{kp_{\text{ave}}}} t^{-1/2}, \tag{3}$$

i.e., p varies linearly with $t^{-1/2}$. This leads to the following data interpretation procedure.

First, the data on the change in pressure p at a given monitoring interval are plotted against the reciprocal of the square root of time $t^{-1/2}$. A straight line should develop for a portion of the data, to which a straight line is fitted. The intersection of this straight line with the time axis $t^{-1/2} = 0$ is denoted by p^* . Then permeability k is obtained from (3) as

$$k_{\text{PP}} = \frac{q\mu}{4\pi R p^*}. \tag{4}$$

Let t^* denote the time at which the straight line crosses the horizontal coordinate, i.e., the time at which $p = 0$. Then porosity ϕ can be found from (3) as

$$\phi_{\text{PP}} = \frac{\pi k p_{\text{ave}} t^*}{\mu R^2} = \frac{q p_{\text{ave}} t^*}{4 R^3 p^*}. \tag{5}$$

2.2. Point-to-line solution

A full solution for cross-hole tests with a point injection ($|L_1L_2| \equiv L = 0$ in Fig. 1) and line monitoring ($|B_1B_2| \equiv B \neq 0$) intervals (a point-to-line solution) has the form [3, Eq. (27)]

$$p_d = \frac{\beta_1}{4} \int_{1/4t_d}^{\infty} \frac{1}{y} \exp[-(1 - \beta_2^2)y] \left\{ \operatorname{erf}\left[\sqrt{y}\left(\beta_2 + \frac{1}{\beta_1}\right)\right] - \operatorname{erf}\left[\sqrt{y}\left(\beta_2 - \frac{1}{\beta_1}\right)\right] \right\} dy, \tag{6}$$

where

$$\beta_1 = \frac{2R}{B}, \quad \beta_2 = \cos \theta_1 \tag{7}$$

and θ_1 is the angle between the line connecting the centroids of the injection and monitoring wells and the monitoring well (see Fig. 1).

A direct asymptotic analysis of (6) is somewhat convoluted. Consider, instead, its time derivative

$$\frac{dp_d}{dt_d} = \frac{\beta_1}{4t_d} \exp\left[-\frac{1 - \beta_2^2}{4t_d}\right] \left\{ \operatorname{erf}\left[\frac{\beta_2 + 1/\beta_1}{2\sqrt{t_d}}\right] - \operatorname{erf}\left[\frac{\beta_2 - 1/\beta_1}{2\sqrt{t_d}}\right] \right\}. \tag{8}$$

Since, for large enough t_d ,

$$\exp\left[-\frac{1 - \beta_2^2}{4t_d}\right] \approx 1 - \frac{1 - \beta_2^2}{4t_d}, \tag{9}$$

$$\operatorname{erf}\left[\frac{\beta_2 + 1/\beta_1}{2\sqrt{t_d}}\right] \approx \frac{1}{\sqrt{\pi}} \frac{\beta_2 + 1/\beta_1}{\sqrt{t_d}},$$

the asymptotic behavior of the pressure derivative (8) is

$$\frac{dp_d}{dt_d} = \frac{1}{2\sqrt{\pi}} t_d^{-3/2}, \tag{10}$$

which is exactly the same as that of the pressure derivative for a point–source solution (3). Integrating (10) yields, for large t_d ,

$$p_d(t_d) = p_d(\infty) - \frac{1}{\sqrt{\pi}} t_d^{-1/2}, \tag{11}$$

where $p_d(\infty)$ is given by [3, Eq. (53)],

$$p_d(\infty) = \frac{\beta_1}{2} \ln \frac{\sqrt{\beta_1^2 + 2\beta_1\beta_2 + 1} + \beta_1\beta_2 + 1}{\sqrt{\beta_1^2 - 2\beta_1\beta_2 + 1} + \beta_1\beta_2 - 1}. \tag{12}$$

Hence the asymptotic late-time behavior of the point source (3) and point-to-line (11) solutions is the same.

An important question is how large the dimensionless time t_d has to be for an asymptotic solution (11) to be an accurate representation of the point-to-line solution (6). This is determined by how accurate the approximations (9) are. They remain accurate, as long as the following conditions hold

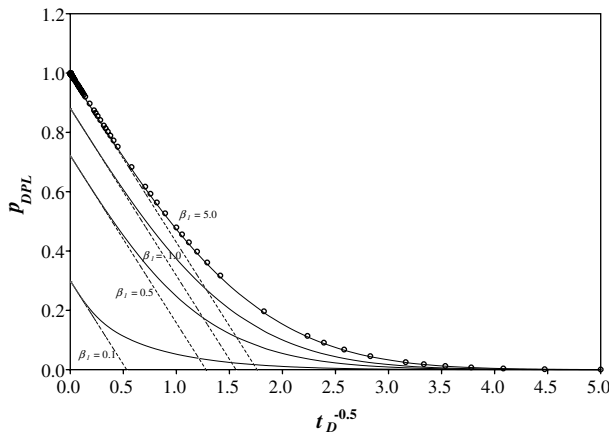


Fig. 2. Dimensionless pressure p_d for point-to-line experiments computed with the full solution (6) (solid curves), its asymptotic counterpart (11) (dashed lines), and the full point-source solution (1) (open circles).

$$t_d \gg \frac{1 - \beta_2^2}{4}, \quad t_d \gg \frac{(\beta_2 \pm 1/\beta_1)^2}{4}. \tag{13}$$

Fig. 2 shows dimensionless pressure $p_d(t_d)$ computed with the full point-to-line solution (6) and its asymptotic counterpart (11), both plotted against $1/\sqrt{t_d}$ for $\beta_2 = 0.01$. This figure also contains the point source solution (1). As β_1 increases, the point source and point-to-line solutions become closer. Fig. 2 reveals that the asymptotic solution (11) provides an accurate approximation of the full solution (6) at intermediate to late dimensionless time t_d , i.e., at small $1/\sqrt{t_d}$. Both the accuracy of this approximation and its range of applicability increase with β_1 . For all practical purposes, the asymptotic solution (11) can be used when $\beta_1 > 0.1$.

To infer equivalent permeability and porosity from pressure data in the monitoring interval, we write (11) in dimensional form,

$$p = \frac{q\mu}{4\pi kR} p_d(\infty) - \frac{q\mu}{4\pi kR} \frac{1}{\sqrt{\pi}} \sqrt{\frac{\phi\mu}{k p_{ave}}} t^{-1/2} \tag{14}$$

and apply the straight line analysis described in the previous section. Let p^* and t^* denote the points at which the straight line (14) crosses the p and $1/\sqrt{t}$ axis, respectively. Then equivalent permeability k_{PL} and porosity ϕ_{PL} are obtained from the asymptotic point-to-line solution (14) as

$$k_{PL} = \frac{q\mu p_d(\infty)}{4\pi R p^*}, \quad \phi_{PL} = \frac{\pi k_{PL} p_{ave} t^* p_d^2(\infty)}{\mu R^2}. \tag{15}$$

2.3. Line-to-line solution

A full solution for cross-hole tests with a line injection ($|L_1 L_2| \equiv L \neq 0$ in Fig. 1) and line monitoring ($|B_1 B_2| \equiv B \neq 0$) intervals (a line-to-line solution) has the form [3, Eq. (35)]

$$p_{dLL} = \frac{1}{4} \int_{1/(4t_d)}^{\infty} \frac{1}{w} \exp[-(1 - \alpha_2^2)w] \times \int_{\lambda=-1}^1 \exp\left\{-\left[\lambda^2 \frac{1-c^2}{\beta_1^2} + 2\lambda \frac{\beta_2 - \alpha_2 c}{\beta_1}\right]w\right\} \times \left\{ \operatorname{erf}\left[\sqrt{w}\left(\alpha_2 + \frac{1}{\alpha_1} + \frac{\lambda c}{\beta_1}\right)\right] - \operatorname{erf}\left[\sqrt{w}\left(\alpha_2 - \frac{1}{\alpha_1} + \frac{\lambda c}{\beta_1}\right)\right] \right\} d\lambda dw. \tag{16}$$

Here dimensionless pressure p_{dLL} is now defined with respect to the length L of the injection interval,

$$p_{dLL} = \frac{4\pi kLp}{q\mu}, \tag{17}$$

β_1 and β_2 are given by (7), and

$$\alpha_1 = \frac{2R}{L}, \quad \alpha_2 = \cos(\pi - \theta_1 - \theta_2), \quad c = \cos \theta_2, \tag{18}$$

where θ_2 is the angle between the injection and monitoring intervals (see Fig. 1).

Following the analysis in previous section, we consider the time derivative of (16)

$$\frac{dp_{dLL}}{dt_d} = \frac{1}{4t_d} \exp\left[-\frac{1 - \alpha_2^2}{4t_d}\right] \times \int_{-1}^1 \exp\left\{-\left[\lambda^2 \frac{1-c^2}{\beta_1^2} + 2\lambda \frac{\beta_2 - \alpha_2 c}{\beta_1}\right]\right\} \times \left\{ \operatorname{erf}\left[\frac{\alpha_2 + 1/\alpha_1 + \lambda c/\beta_1}{2\sqrt{t_d}}\right] - \operatorname{erf}\left[\frac{\alpha_2 - 1/\alpha_1 + \lambda c/\beta_1}{2\sqrt{t_d}}\right] \right\} d\lambda. \tag{19}$$

For large enough t_d ,

$$\exp\left[-\frac{1 - \alpha_2^2}{4t_d}\right] \approx 1 - \frac{1 - \alpha_2^2}{4t_d}, \tag{20}$$

$$\operatorname{erf}\left[\frac{A}{2\sqrt{t_d}}\right] \approx \frac{1}{\sqrt{\pi}} \frac{A}{\sqrt{t_d}},$$

so that the leading term in the expansion of (19) is

$$\frac{dp_{dLL}}{dt_d} = \frac{\mathcal{J}}{4\alpha_1 \sqrt{\pi}} t_d^{-3/2}, \tag{21}$$

where

$$\mathcal{J} = 2 \int_{-1}^1 \exp\left\{-\left[\lambda^2 \frac{1-c^2}{\beta_1^2} + 2\lambda \frac{\beta_2 - \alpha_2 c}{\beta_1}\right]\right\} d\lambda. \tag{22}$$

Evaluating (22) yields

$$\mathcal{J} = \frac{\beta_1}{\sqrt{1-c^2}} e^{A^2} \left[\operatorname{erf}\left(A + \frac{\sqrt{1-c^2}}{\beta_1}\right) - \operatorname{erf}\left(A - \frac{\sqrt{1-c^2}}{\beta_1}\right) \right], \tag{23a}$$

$$A = \frac{\beta_2 - \alpha_2 c}{\sqrt{1-c^2}}$$

for $c \neq 1$, and

$$\mathcal{F} = \frac{\beta_1}{\beta_2 - \alpha_2} \left[\exp\left(2\frac{\beta_2 - \alpha_2}{\beta_1}\right) - \exp\left(-2\frac{\beta_2 - \alpha_2}{\beta_1}\right) \right] \quad (23b)$$

for $c = 1$. Similar to the point–source (3) and point-to-line (10) solutions, the pressure derivative (21) in the line-to-line solution decays with time at the rate $t_d^{-3/2}$.

The integration of (21) yields the asymptotic behavior of dimensionless pressure at large dimensional time

$$p_{dLL}(t_d) = p_{dLL}(\infty) - \frac{\mathcal{F}}{2\alpha_1} t_d^{-1/2}, \quad (24)$$

where [3, Eq. (54)]

$$p_{dLL}(\infty) = \frac{1}{2} \int_{-1}^1 \ln \left[\frac{\left\{ \sqrt{\frac{\alpha_1^2 \lambda^2}{\beta_1^2} + 2\lambda \frac{\alpha_1^2 \beta_2 + \alpha_1 c}{\beta_1} + \alpha_1^2 + 2\alpha_1 \alpha_2 + 1 + \alpha_1 \alpha_2 + 1 + \frac{\alpha_1 c \lambda}{\beta_1}} \right\}}{\left\{ \sqrt{\frac{\alpha_1^2 \lambda^2}{\beta_1^2} + 2\lambda \frac{\alpha_1^2 \beta_2 - \alpha_1 c}{\beta_1} + \alpha_1^2 - 2\alpha_1 \alpha_2 + 1 + \alpha_1 \alpha_2 - 1 + \frac{\alpha_1 c \lambda}{\beta_1}} \right\}} \right] d\lambda \quad (25)$$

is the steady-state solution for line-injection/line-monitoring experiments.

Hence the line-to-line solution (16) has the same asymptotic behavior (24) as its point–source (1) and point-to-line (6) counterparts, i.e., in all three tests dimensionless pressure varies linearly with $1/\sqrt{t_d}$ for large enough values of dimensionless time t_d . Such a temporal scaling is to be expected and follows immediately from the scaling properties of diffusion equation, which underlines the full solutions (1), (6) and (16).

The accuracy of the asymptotic solution (24) depends on the accuracy of expansions (20). This leads to the following constraints on the duration of a pumping test,

$$t_d \gg \frac{1 - \alpha_2^2}{4}, \quad t_d \gg \frac{(\alpha_2 \pm 1/\alpha_1 + \lambda c/\beta_1)^2}{4}. \quad (26)$$

These relationships provide useful guidelines for the design and interpretation of cross-hole pumping tests.

Fig. 3 compares dimensionless pressure p_{dLL} computed with the full solution (16) and its asymptotic counterpart (24). For the purpose of data analysis, the two solutions are identical for intermediate to late dimensionless time (small $1/\sqrt{t_d}$), with the correspondence improving as $\alpha_1 = \beta_1$ increase. The approximation can be used to infer hydraulic parameters from line-to-line pumping tests when $\alpha_1 = \beta_1 > 0.2$.

To infer equivalent permeability and porosity from pressure data in the monitoring interval, we write (24) in its dimensional form,

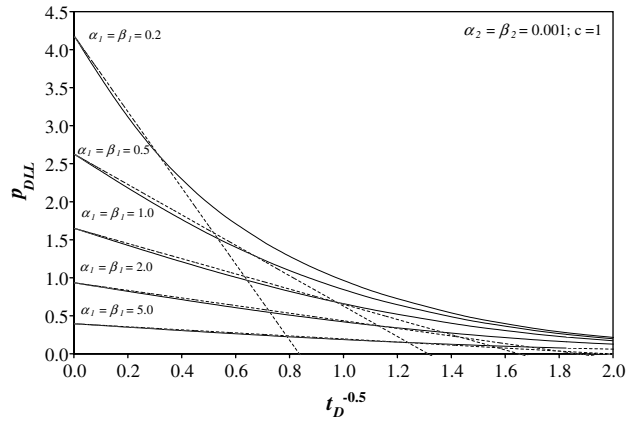


Fig. 3. Dimensionless pressure p_{dLL} for line-to-line experiments computed with the full solution (16) (solid curves) and its asymptotic counterpart (24) (dashed lines).

$$p = \frac{q\mu}{4\pi kL} p_{dLL}(\infty) - \frac{q\mu r}{4\pi kL} \frac{\mathcal{F}}{2\alpha_1} \sqrt{\frac{\phi\mu}{kp_{ave}}} t^{-1/2} \quad (27)$$

and apply the straight line analysis. Let p^* and t^* denote the points at which the straight line (14) crosses the p and $1/\sqrt{t}$ axis, respectively. Then equivalent permeability k_{LL} and porosity ϕ_{LL} are obtained from the asymptotic point-to-line solution (27) as

$$k_{LL} = \frac{q\mu}{4\pi L p^*} p_{dLL}(\infty), \quad \phi_{LL} = \frac{kp_{ave} t^*}{\mu r^2} \frac{4\alpha_1^2}{\mathcal{F}^2} p_{dLL}^2(\infty). \quad (28)$$

3. Application to pressure interference tests in unsaturated fractured tuffs

We apply our technique to infer permeability and porosity from three-dimensional pressure interference tests conducted at the Apache Leap Research Site (ALRS). These tests employed the point–source, point-injection/line-observation, and line-injection/line-observation configurations.

3.1. Site and test description

The test site is located near Superior, Arizona at an elevation of 1200 m above sea level. It consists of 22 vertical and inclined (at 45°) boreholes that have been completed to a maximum depth of 30 m within a geologically

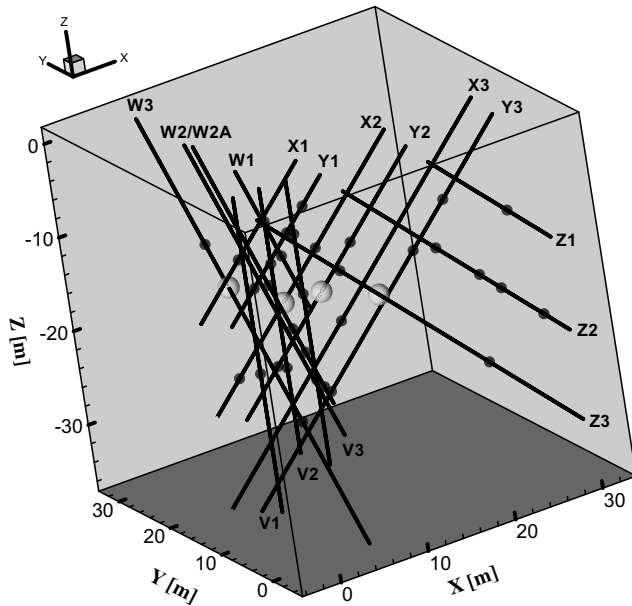


Fig. 4. Three-dimensional perspective view of boreholes (solid black-lines), with centroids of injection (larger gray spheres) and observation (small black spheres) intervals shown for selected cross-hole tests at the ALRS.

distinct unit of partially welded unsaturated tuff. Fig. 4 shows three-dimensional perspective view of the 16 of the 22 boreholes at the site. On this figure centroids of injection (larger gray spheres) and observation intervals (small black spheres) are shown for selected cross-hole tests. The upper 1.8 m of each borehole is cased. Core samples were taken from 9 of the 22 boreholes and a variety of tests were performed [10] to determine the interstitial properties of the tuff matrix. Single-hole pneumatic and hydraulic injection tests with various injection interval lengths were conducted [10,11] to determine the permeabilities of the fractured tuff. Additional details on these tests and the site can be found in [4,5].

Core and single-hole pneumatic injection tests provide information only about a small volume of rock in the close vicinity of the injection interval. Fractured rock properties measured on such small scales tend to vary erratically in space rendering the rock strongly heterogeneous. To determine the properties of the rock on larger scales and to estimate the degree to which fractures are pneumatically interconnected, numerous cross-hole pneumatic injection tests were conducted [4,5] between 16 boreholes (one of which included all 22 boreholes), 11 of which have been previously subjected to single-hole testing.

In a pneumatic cross-hole test, air is injected into an isolated interval within one borehole and pressure responses are monitored in isolated intervals within this and all other boreholes. The tests were performed using modular straddle packer systems that were readily adaptable to various test configurations and allow for rapid replacement of failed components, modification

of the number of packers, and adjustment of distances between them in both the injection and monitoring boreholes. The main injection string consisted of three packers, one of which was located near the soil surface to isolate the borehole from the atmosphere, while the remaining two enclosed the injection interval. To minimize borehole storage effects, the air-filled volume of the injection interval was made relatively small.

A typical cross-hole test consisted of packer inflation, a period of pressure recovery, air injection and another period of pressure recovery. Once packer inflation pressure had dissipated in all (monitoring and injection) intervals, air injection at a constant flow rate commenced. It generally took several days for pressure in most monitoring intervals to stabilize. In some tests, injection pressure was allowed to dissipate until ambient conditions have been recovered. In other tests, air injection continued at incremental flow rates, each lasting until the corresponding pressure had stabilized, before the system was allowed to recover.

Three types of cross-hole tests were conducted at the ALRS in three phases. Phase 1 included line-injection/line-monitoring (LL) tests, in which injection and monitoring took place along a large portion of the borehole that had been isolated from the atmosphere by means of shallow packers. Some of the boreholes were open to the atmosphere. Phase 2 consisted of point-injection/line-monitoring (PL) tests, in which air was injected into a 2 m section in one borehole and pressure was recorded along the entire length of each monitoring borehole. In Phase 3, we conducted point-injection/point-monitoring (PP) tests in which both the injection and many monitoring intervals were short enough to be treated as points for purposes of type-curve analysis [6]. All of the boreholes were packed off during the PL and PP tests. A total of 44 cross-hole pneumatic interference tests of various types (constant injection rate, multiple

Table 1

Test name, name of injection borehole, upper and lower extent of injection interval measured along borehole from lower lip of casing, injection flow rate (Q), and injection interval permeability computed by means of a steady-state formula given in [11]

Test name	Injection borehole	Injection interval [m]	Q [slpm]	k [m ²]
LL2	Y2	10.0–30.0	101.2	8.83×10^{-15}
PL3	Y2	15.0–17.0	20	4.10×10^{-14}
PL4	Y2	21.0–23.0	1	2.64×10^{-15}
PL8	Y2	18.0–20.0	1	3.03×10^{-15}
PL9	Y2	26.0–28.0	1	1.08×10^{-15}
PL10	Y2	23.0–25.0	1	1.51×10^{-15}
PL15	Y2	21.0–23.0	1	2.29×10^{-15}
PP4	Y2	15.0–17.0	50.0	5.55×10^{-14}
PP5	X2	18.5–20.7	5.0	5.13×10^{-15}
PP6	Z3	15.9–17.9	5.0	1.06×10^{-14}
PP7	W3	19.2–20.4	5.0	2.25×10^{-14}
PP8	Y2	15.0–17.0	50.0	5.37×10^{-14}

step injection rates, instantaneous injection) were conducted using various configurations of injection and monitoring intervals (LL, PL and PP).

3.2. Results

We use our asymptotic approach to analyze data sets collected from 12 cross-hole tests, whose identifiers are listed in Table 1 together with the identifiers of injection boreholes, upper and lower extent of injection intervals,

and injection flow rates q . Much of the data collected from these tests were analyzed earlier by means of a steady-state analysis [1], type curves [6], and a three-dimensional numerical inverse model [7,12]. Table 1 also contains the estimates of equivalent permeability obtained from the steady-state analysis [1] at the injection interval.

Fig. 5 shows six typical data sets obtained from several cross-hole tests with point-injection/line-observation configurations. All data sets share a similar

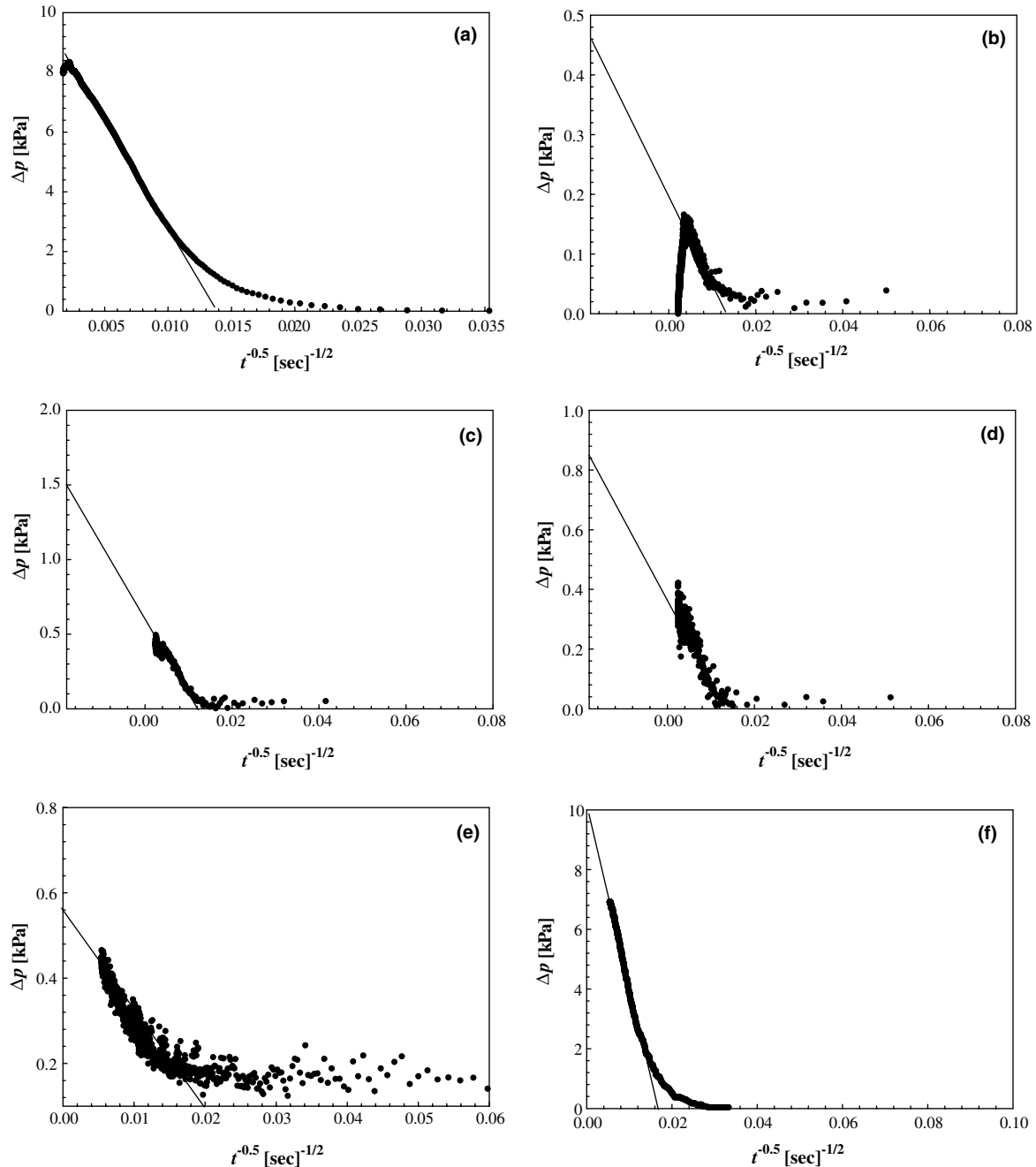


Fig. 5. Pressure data plotted against the inverse of the square root of time $1/\sqrt{t}$ obtained from the point-to-line tests in the monitoring intervals: (a) V1 during test PP4, (b) Z1 during test PP4, (c) W1 during test PP5, (d) X1 during PP5, (e) W1 during test PP7, and (f) W3U during test PP7. Straight line (11) is fitted to all six data sets.

behavior, which was predicted by our asymptotic analysis in the previous section. Indeed, after early times, during which pressure responses may be dominated by borehole storage, skin, and local heterogeneity, pressure data fall on a straight line when plotted against $1/\sqrt{t}$. A slight deviation from the straight-line behavior in Fig. 5a and b can be explained by the decline in barometric pressure [6], but a straight line develops prior to the pressure decline. While some of the data sets (e.g., Fig. 5a and f) are characterized by high signal-to-noise ratios, in others (e.g., Fig. 5b-e) this ratio was relatively small. While small signal-to-noise ratios severely compromise the fidelity of traditional approaches, such as type-curve and steady-state analyses, our asymptotic approach remains quite robust.

Fig. 6 demonstrates similar behavior of pressure data collected from two cross-hole tests with line-injection/line-observation configurations.

Table 2 summarizes the statistics of log permeability $\log_{10}k$ and log porosity $\log_{10}\phi$ obtained by the asymptotic approach using the point-source, point-to-line and line-to-line solutions. The values of $\log_{10}k$ vary from -15.14 to -12.38 , with the mean -13.72 , variance 0.25 , and the coefficient of variation -0.037 . The values of $\log_{10}\phi$ range from -3.70 to -0.24 , with the mean -1.78 , variance 0.41 , and the coefficient of variation -0.361 . These statistics include the estimates of equivalent permeability and porosity obtained from the point-source tests reported in [2].

The analysis of these data reveal that while the mean values of both permeability and porosity inferred from the three types of cross-hole test are more or less the same, the corresponding variances increase from the point-source to point-to-line and line-to-line cases. This implies that the variability of equivalent parameters increases with the support volume of cross-hole tests, i.e., with the length of injection and observation intervals. This unexpected finding might be an indication of

Table 2

Summary statistics of $\log_{10}k$ [m^2] and $\log_{10}\phi$ obtained by the asymptotic straight line method

Applicable solution	Sample size	$\log_{10}k$ [m^2]		$\log_{10}\phi$	
		Mean	Variance	Mean	Variance
Point source	46	-13.65	0.20	-1.69	0.21
Point-line	93	-13.78	0.32	-1.86	0.26
Line-line	8	-13.60	0.37	-1.49	0.72

Table 3

Summary statistics of $\log_{10}k$ [m^2] and $\log_{10}\phi$ obtained by the asymptotic straight line method for each test

Test	Sample size	$\log_{10}k$ [m^2]		$\log_{10}\phi$	
		Mean	Variance	Mean	Variance
LL2	8	-13.60	0.37	-1.49	0.72
PL3	12	-13.68	0.19	-1.73	0.68
PL4, PL8, PL9, PL10, PL15	13	-14.10	0.16	-1.72	0.51
PP4	31	-13.49	0.32	-1.54	0.23
PP5	20	-13.84	0.30	-1.60	0.43
PP6	19	-13.85	0.04	-2.48	0.18
PP7	15	-13.96	0.05	-2.10	0.04
PP8	29	-13.55	0.27	-1.65	0.30

the fractal nature of fractured tuff at the ALRS. It can also be an artifact caused by the smaller number of samples for the line-line case.

Table 3 separates the statistics of log permeability $\log_{10}k$ and log porosity $\log_{10}\phi$ by the test. (Because the number of data available for tests PL4, PL8, PL9, PL10, and PL15 are small, the statistics of these data are reported together.) In general, the equivalent permeabilities and porosities obtained from tests conducted with injection at higher permeability intervals (see Table 1) are higher than those with injection taking place at intervals with lower permeabilities. The variances of both permeability and porosity are higher for the tests with injections through intervals of high permeability.

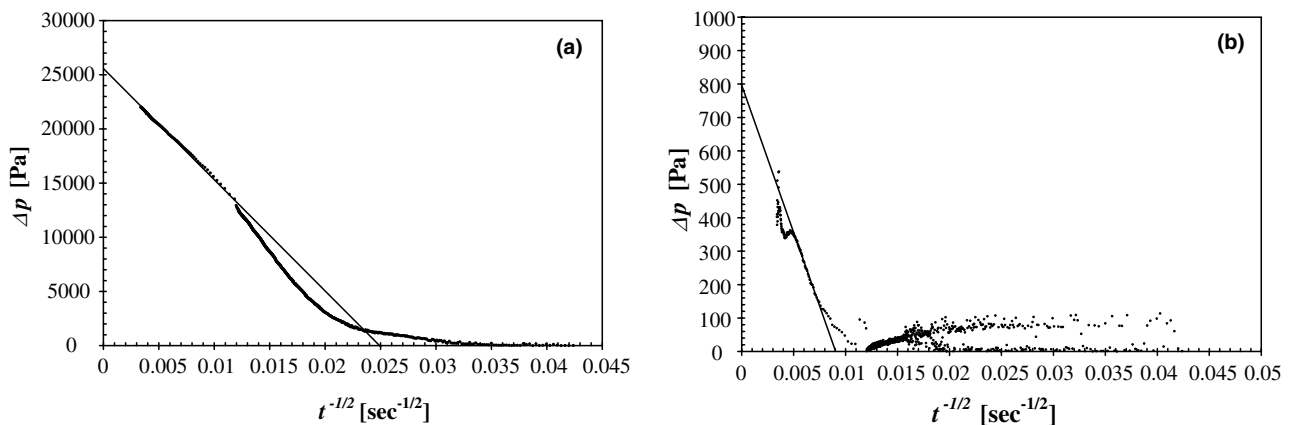


Fig. 6. Pressure data plotted against the inverse of the square root of time $1/\sqrt{t}$ obtained from the line-to-line tests in monitoring intervals: (a) V2 during test LL2 and (b) Z2 during test LL2. Straight line (24) is fitted to both data sets.

It is interesting to note that the variance of porosity is on average larger than the variance of permeability.

Since the rock is highly heterogeneous, the estimates of permeability and porosity vary from one test to another. Therefore, the rock can only be tested thoroughly through cross-hole tests conducted in a tomographic manner (meaning that injection took place at different locations throughout the rock mass while monitoring took place in all neighboring intervals simultaneously).

Fig. 7 depicts a histogram of log permeability $\log_{10}k$ inferred from all tests analyzed with the point–source, point–line, and the line–line solutions. Log permeability has a bimodal distribution, in which one mode corresponds to a few dominant fractures with high permeability and the other mode corresponds to less permeable fractures, with a smaller value of permeability consisting another peak.

Fig. 8 depicts a histogram of log porosity $\log_{10}\phi$ inferred from all tests analyzed with the point–source, point–line, and the line–line solutions. Unlike permeability in Fig. 6, porosity has a unimodal distribution, which might be due to the fact that porosity is a quantity averaged over multiple sets of fractures.

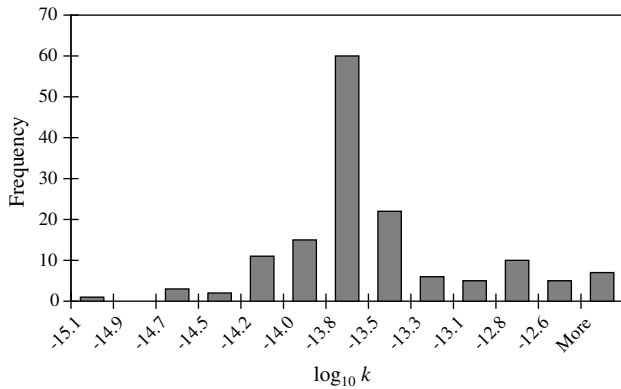


Fig. 7. Histogram of log permeability $\log_{10}k$ inferred with the asymptotic analysis from the point–source, point-to-line, and line-to-line tests.

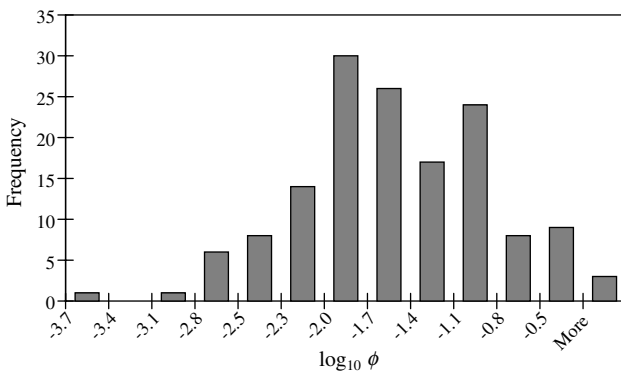


Fig. 8. Histogram of log porosity $\log_{10}\phi$ inferred with the asymptotic analysis from the point–source, point-to-line, and line-to-line tests.

4. Comparison with alternative data interpretation techniques

To ascertain the accuracy and robustness of our asymptotic approach to data analysis, we compare the estimates of permeability and porosity obtained in the previous section with those derived elsewhere by means of a type-curve [6], steady-state [1], and numerical inverse [7,12] analyses.

4.1. Type-curve analysis

Data from a cross-hole pneumatic injection test (labeled PP4) were analyzed in [6] by means of a type-curve analysis. In this analysis, the type curves (1) were generalized to account for the combined effects of compressible air storage and skin in monitoring intervals. (The data derived from the PP4 test suggest that air compressibility is the dominant factor affecting single-hole pneumatic injection tests, while the skin effect is negligible [8].) To accentuate phenomena such as the effect of barometric pressure, and to constrain the estimation of pneumatic parameters, the type-curve analysis [6] relied on both pressure and pressure derivatives plotted against the logarithm of time. A further improvement in estimation of pneumatic rock properties was achieved by developing type curves that allowed for a simultaneous analysis of pressure buildup and recovery data [6].

Fig. 9 demonstrates an excellent agreement between the equivalent permeabilities inferred from the PP4 cross-hole test by means of both type-curve [6] and asymptotic analyses. A similar comparison for equivalent porosity in Fig. 10 shows that while the agreement between the two estimates is generally good, a few type-curve estimates are heavily biased towards lower values. This discrepancy comes from the data collected in the monitoring intervals of boreholes Y3, Z2 and

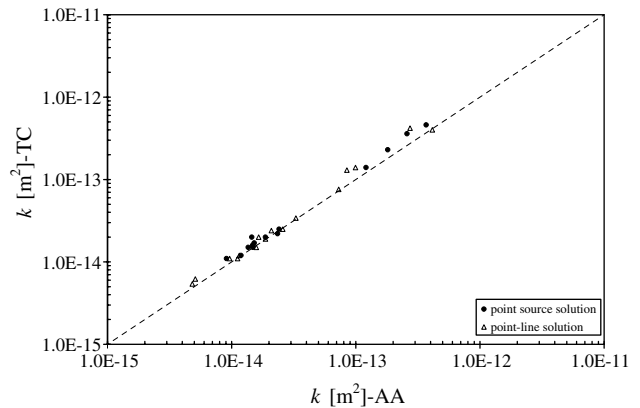


Fig. 9. Comparison of permeabilities inferred from test PP4 by means of the asymptotic (AA) and type-curve (TC) analyses. Data from both the point–source ($\beta_1 \geq 5$) and point-to-line ($\beta_1 < 5$) test configurations (denoted by closed circles and open triangles, respectively) were used.

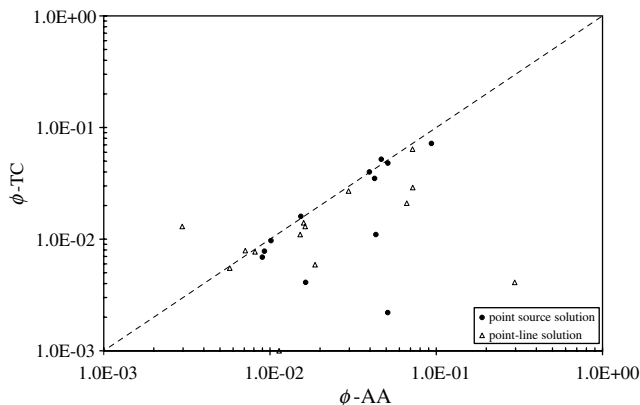


Fig. 10. Comparison of porosities inferred from test PP4 by means of the asymptotic (AA) and type-curve (TC) analyses. Data from both the point–source ($\beta_1 \geq 5$) and point-to-line ($\beta_1 < 5$) test configurations (denoted by closed circles and open triangles, respectively) were used.

Z3. The type-curve interpretation of these data [6, Fig. 10j] assumed a very high observation wellbore storage, which might have caused the porosity estimates to be artificially small. Since the asymptotic analysis relies on the intermediate to late data, it is not affected by wellbore storage. Consequently, it yields the estimates of porosity that are more consistent with those obtained with the numerical inverse interpretation, which is discussed in Section 4.3. Another factor that can lead to nonunique estimates of porosity is the lack of match between the type-curve and early time data [2].

4.2. Steady-state analysis

The inability to analyze many cross-hole test data by means of analytically derived type curves led Illman and Neuman [1] to use a steady-state formula [3] for hydraulic cross-hole tests in saturated rocks. They found that their steady-state approach works well for pressure records whose signal-to-noise ratio is too low to allow for a meaningful transient analysis. Though the steady-state method does not yield estimates of porosity, it does yield reliable estimates of permeability between an injection and a monitoring interval.

Fig. 11 contains the estimates of equivalent permeability obtained with the steady-state [1] and asymptotic analyses. The agreement between the two is quite good with a slight bias towards the steady-state estimates. This may be due to the fact that the steady-state estimates are associated with larger support volumes of the rock. Pumping tests in fractured carbonates revealed a similar time dependence of permeability [13].

4.3. Numerical inverse analysis

The three-dimensional numerical inverse analysis [7,12] consisted of two phases. In the first phase, data were analyzed one pressure record at a time, which is

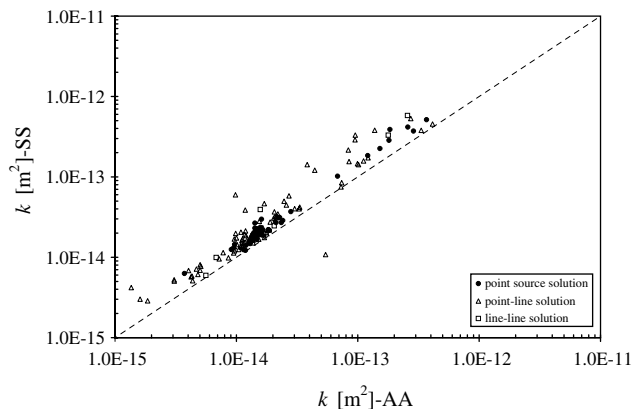


Fig. 11. Comparison of permeabilities inferred from tests PP4–PP8 and LL2 by means of the asymptotic (AA) and steady-state (SS) analyses. For tests PP4–PP8, data from both the point–source ($\beta_1 \geq 5$) and point-to-line ($\beta_1 < 5$) test configurations (denoted by closed circles and open triangles, respectively) were used. Test LL2 (open squares) consists of line-injection and line-monitoring.

conceptually analogous to analytical interpretation techniques described above. In the second phase, the same data were analyzed simultaneously in a tomographic manner. Pressure records were filtered to isolate the responses due primarily to air injection, which significantly reduced the size of a data set without the significant loss of information. This was accomplished by ignoring the portions of pressure records that were strongly influenced by barometric pressure fluctuations and/or other extraneous phenomena and by representing the remaining portions via a relatively small number of “match points.” To capture with equal fidelity both rapid pressure transients at early time and more gradual pressure variations at later time, these match points were distributed more or less evenly along the log-transformed time axis. Matching was done with equal weighting using the match points with the numerical inverse interpretation.

Fig. 12 compares the estimates of permeability obtained with the asymptotic analysis and the inverse model that treated the medium as homogeneous. The agreement is generally good, but it is characterized by a greater scatter than the agreement between the asymptotic and type-curve estimates in Fig. 8.

Fig. 13 provides a similar comparison for the estimates of porosity. There is a much larger scatter reflecting the fact that the porosity estimates are more uncertain. This is also reflected in the wider confidence intervals associated with the porosity estimates in comparison to the permeability estimates by means of the numerical inverse model [7,12].

4.4. Advantages of the asymptotic approach

The proposed asymptotic approach overcomes many difficulties and limitations encountered in existing steady-state and transient approaches to obtaining reliable

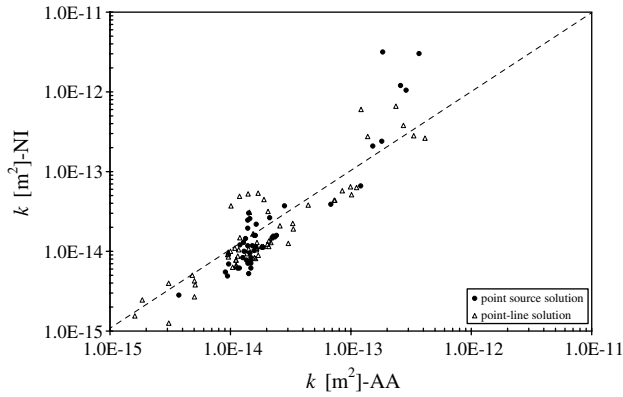


Fig. 12. Comparison of permeabilities inferred from tests PP4–PP8 by means of the asymptotic (AA) and numerical inverse (NI) analyses. Data from both the point–source ($\beta_1 \geq 5$) and point-to-line ($\beta_1 < 5$) test configurations (denoted by closed circles and open triangles, respectively) were used.

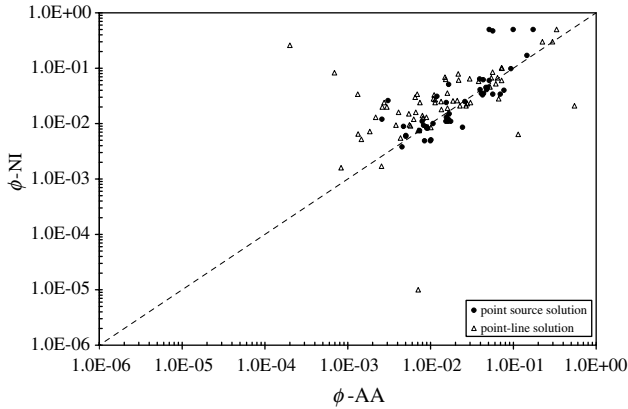


Fig. 13. Comparison of porosities inferred from tests PP4–PP8 by means of the asymptotic (AA) and numerical inverse (NI) analyses. Data from both the point–source ($\beta_1 \geq 5$) and point-to-line ($\beta_1 < 5$) test configurations (denoted by closed circles and open triangles, respectively) were used.

estimates of equivalent permeability and porosity. In particular,

- Unlike steady-state techniques, it yields estimates of both permeabilities and porosities and is not based on an often hard to verify assumption that a pressure interference test reaches a steady state;
- It is much easier to conduct than either transient type-curve or numerical inverse analyses, both of which have therefore been limited to relatively few single- and cross-hole tests;
- It works well for pressure records whose signal-to-noise ratio is too low to allow for a meaningful transient analysis. This also includes cases when pressure transients are heavily affected by borehole storage, external forcings, and heterogeneities that cause the data to depart from analytically derived type-curve models;

- It eliminates the subjective fitting of data to type curves. The latter approach requires considerable experience by the hydrogeologist and the results are heavily dependent on the analyst.

5. Correlation between permeability and porosity

To compute correlations between the permeability and porosity inferred from test PP4, Kriged and pilot point estimates of $\log_{10}\phi$ were plotted against the corresponding estimates of $\log_{10}k$ and regression was used to fit a straight line to these data [12]. This procedure resulted in relatively low correlation coefficients R^2 for both Kriged ($R^2 = 0.428$) and pilot point ($R^2 = 0.463$) estimates. A hypothesis that the observed scatter can be explained by a linear trend did not pass a standard Fisher test. Such weak linear correlations may be due in part to the effect of correlated estimation errors on the scatter. The slope of the regression line is 0.522 ± 0.004 for Kriged estimates and 0.247 ± 0.174 for the pilot point estimates. This is equivalent to a 1:2 linear relationship between $\log_{10}\phi$ and $\log_{10}k$ based on Kriged estimates and a 1:4 linear relationship based on the pilot point estimates.

These correlations were compared with a compilation of the correlation coefficients found in saturated fractured rocks worldwide [14]. The latter were analyzed together to yield the slopes of 0.28 and 0.35 for the Kriged and pilot-point regression lines between log porosity and log permeability, respectively. These are roughly equivalent to a 1:3 linear relationship between the two parameters.

Fig. 14 provides a similar correlation analysis of the estimates of equivalent permeabilities and porosities inferred by the asymptotic analysis from the data collected at the ALRS. It yields correlation coefficient $R^2 = 0.43$ and the slope of the regression line 0.84, which results

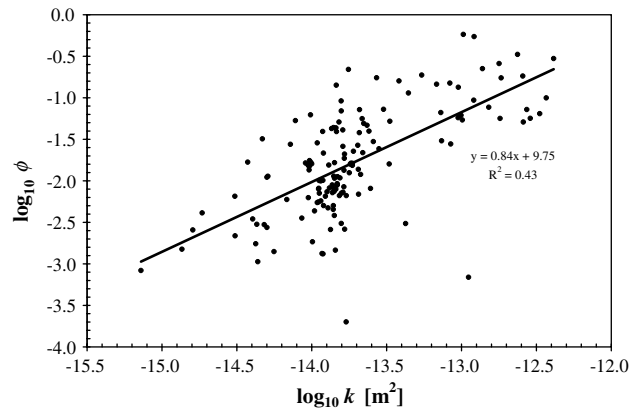


Fig. 14. Correlation between log conductivity $\log_{10}k$ and log porosity $\log_{10}\phi$.

in a less than 1:1 linear relationship between $\log_{10}\phi$ and $\log_{10}k$. The discrepancy between our present findings and those reported in [12] is due to the differences in the data interpretation. While the present analysis treats the rock as uniform on the scale of the measurement, the analysis in [12] assumes that the rock can be modeled as a random fractal with a power variogram. Another possible explanation is that more data are incorporated in the present analysis.

6. Conclusions

This study leads to the following major conclusions:

- (1) We developed a set of asymptotic approximations for the cross-hole pneumatic injection tests. These expressions allow one to infer the equivalent permeability and porosity of unsaturated fractured rocks by means of a straight-line analysis when pressure data are plotted against the inverse of the square root of time $1/\sqrt{t}$.
- (2) These solutions are valid, and the data interpretation technique should be used, for intermediate to late times t . We provided a set of conditions that quantify these times in terms of the geometric parameters of the test, such as the lengths of injection and monitoring intervals and the angles between them.
- (3) The asymptotic analysis was used to interpret multiple cross-hole pneumatic injection tests in unsaturated fractured tuff at the Apache Leap Research Site (ALRS) in Superior, Arizona. The obtained estimates of equivalent permeability and porosity were compared with those derived previously by means of the type-curve, steady-state, and numerical inverse analyses. This comparison demonstrates that the asymptotic analysis yields reliable estimates of the rock properties, while being significantly easier to administer than the existing alternatives.
- (4) A key advantage of the asymptotic analysis over its steady-state counterpart is that the former yields reliable estimates of both equivalent permeability and porosity between an injection and a monitoring interval, while the latter yields only equivalent permeability. Also, it does not require for the pumping tests to reach a steady state, which is often problematic.
- (5) The asymptotic analysis of data remains robust even when applied to pressure records, whose signal-to-noise ratio is too low to allow for meaningful transient type-curve analyses. This enabled us to augment in a significant way the existing database of permeabilities and porosities at the ALRS.
- (6) Even though the asymptotic analysis treats the rock as pneumatically uniform and isotropic on the scale of measurement, it ultimately yields information about the spatial, scale, and directional dependence of pneumatic connectivity, permeability and porosity of fractures across the site on scales relevant to the cross-hole test.
- (7) We found a correlation between the estimates of permeability and porosity at the ALRS. Similar correlations have been observed at other sites worldwide.

Acknowledgement

The first author was supported in part by the 2003 Old Gold Fellowship from the University of Iowa, as well as by funding from the National Science Foundation (NSF) under Grand no. 0229713 and the Strategic Environmental Research & Development Program (SERDP). The research by the second author was performed at Los Alamos National Laboratory under the auspices of the US Department of Energy, contract W-7405-ENG-36; and was supported by the LDRD Program at Los Alamos National Laboratory.

References

- [1] Illman WA, Neuman SP. Steady-state analyses of cross-hole pneumatic injection tests in unsaturated fractured tuff. *J Hydrol* 2003;281:36–54.
- [2] Illman WA, Tartakovsky DM. Asymptotic analysis of three-dimensional pressure interference tests: a point-source solution. *Water Resour Res* 2005;41:W01002. doi:10.1029/2004WR003431.
- [3] Hsieh PA, Neuman SP. Field determination of the three-dimensional hydraulic conductivity tensor of anisotropic media, 1. Theory. *Water Resour Res* 1985;21(11):1655–65.
- [4] Illman WA, Thompson DL, Vesselinov VV, Chen G, Neuman SP. Single- and cross-hole pneumatic tests in unsaturated fractured tuffs at the apache leap research site: phenomenology, spatial variability, connectivity and scale. Tech Rep NUREG/CR-5559, US Nucl Regul Comm, Washington DC, 1998.
- [5] Illman WA. Single- and cross-hole pneumatic injection tests in unsaturated fractured tuffs at the Apache Leap Research Site near Superior, Arizona. PhD thesis, Dep of Hydrol and Water Resour, University of Arizona, Tucson, 1999.
- [6] Illman WA, Neuman SP. Type-curve interpretation of a cross-hole pneumatic test in unsaturated fractured tuff. *Water Resour Res* 2001;37(3):583–604.
- [7] Vesselinov VV, Neuman SP, Illman WA. Three-dimensional numerical inversion of pneumatic cross-hole tests in unsaturated fractured tuff: 1. Methodology and borehole effects. *Water Resour Res* 2001;37(12):3001–17.
- [8] Illman WA, Neuman SP. Type-curve interpretation of multi-rate single-hole pneumatic injection tests in unsaturated fractured rock. *Ground Water* 2000;38(6):899–911.
- [9] Cooper HH, Jacob CE. A generalized graphical method for evaluating formation constants and summarizing well field history. *EOS Trans* 1946;27:526–34.
- [10] Rasmussen TC, Evans DD, Sheets PJ, Blanford JH. Unsaturated fractured rock characterization methods and data sets at the

- Apache Leap tuff site. Tech Rep NUREG/CR-5596, US Nucl Regul Comm, Washington DC, 1990.
- [11] Guzman AG, Geddis AM, Henrich MJ, Lohrstorfer CF, Neuman SP. Summary of air permeability data from single-hole injection tests in unsaturated fractured tuffs at the Apache Leap Research Site: Results of steady-state test interpretation. Tech Rep NUREG/CR-6360, US Nucl Regul Comm, Washington DC, 1996.
- [12] Vesselinov VV, Neuman SP, Illman WA. Three-dimensional numerical inversion of pneumatic cross-hole tests in unsaturated fractured tuff: 2. Equivalent parameters, high-resolution stochastic imaging and scale effects. *Water Resour Res* 2001;37(12): 3019–41.
- [13] Schulze-Makuch D, Cherkauer DS. Variations in hydraulic conductivity with scale of measurement during aquifer tests in heterogeneous, porous carbonate rocks. *Hydrogeol J* 1998;6: 204–15.
- [14] Guimera J, Carrera J. A comparison of hydraulic and transport parameters measured in low permeability fractured media. *J Cont Hydrol* 2000;41:261–81.